

Tensile behaviour of 9Cr–1Mo tempered martensitic steels irradiated up to 20 dpa in a spallation environment

J. Henry, X. Averty, Y. Dai, J. P. Pizzanelli

▶ **To cite this version:**

J. Henry, X. Averty, Y. Dai, J. P. Pizzanelli. Tensile behaviour of 9Cr–1Mo tempered martensitic steels irradiated up to 20 dpa in a spallation environment. Journal of Nuclear Materials, 2008, 377 (1), pp.80-93. 10.1016/j.jnucmat.2008.02.027 . cea-02355774

HAL Id: cea-02355774

https://cea.hal.science/cea-02355774

Submitted on 4 Oct 2022

HAL is a multi-disciplinary open access archive for the deposit and dissemination of scientific research documents, whether they are published or not. The documents may come from teaching and research institutions in France or abroad, or from public or private research centers.

L'archive ouverte pluridisciplinaire **HAL**, est destinée au dépôt et à la diffusion de documents scientifiques de niveau recherche, publiés ou non, émanant des établissements d'enseignement et de recherche français ou étrangers, des laboratoires publics ou privés.



Distributed under a Creative Commons Attribution 4.0 International License

Tensile behaviour of 9Cr–1Mo tempered martensitic steels irradiated up to 20 dpa in a spallation environment

J. Henry [a,*], X. Averty [c], Y. Dai [b], J.P. Pizzanelli [c]

[a] *CEA Saclay, SRMA, F-91 191 Gif-sur-Yvette cedex, France*
[b] *Spallation Source Division, Paul Scherrer Institut, CH-5232 Villingen, Switzerland*
[c] *CEA Saclay, SEMI, F-91 191 Gif-sur-Yvette cedex, France*

Tensile specimens of 9Cr–1Mo (EM10) and mod 9Cr–1Mo (T91) martensitic steels in the normalized and tempered metallurgical conditions were irradiated with high energy protons and neutrons up to 20 dpa at average temperatures up to about 360 °C. Tensile tests were carried out at room temperature and 250 °C and a few samples were tested at 350 °C. The fracture surfaces of selected specimens were characterized by Scanning Electron Microscopy (SEM). While all irradiated specimens displayed at room temperature considerable hardening and loss of ductility, those irradiated to doses above approximately 16 dpa exhibited a fully brittle behaviour and the SEM observations revealed significant amounts of intergranular fracture. Helium accumulation, up to about 0.18 at.% in the specimens irradiated to 20 dpa, is believed to be one of the main factors which triggered the brittle behaviour and intergranular fracture mode. One EM10 and one T91 specimen irradiated to 20 dpa were annealed at 700 °C for 1 h following irradiation and subsequently tensile tested. In both cases, a remarkable recovery of ductility and strain-hardening capacity was observed after annealing, while the strength remained significantly above that of the unirradiated material.

1. Introduction

Ferritic/martensitic steels are candidate materials for the liquid metal containers of future high power spallation sources or for the first wall blankets of fusion reactors. In both cases, the structural materials will experience extensive radiation damage together with the production of high quantities of transmutation induced impurities, notably helium and hydrogen. In order to characterize the effects of such specific irradiation conditions on the mechanical properties, an irradiation programme is being conducted using the SINQ spallation targets. Following the first SINQ target irradiation programme (STIP I) [1], a second irradiation, STIP II, was carried out in 2001–2002 [2]. As part of the CEA contribution to the STIP international collaboration, 9Cr–1Mo (EM10 steel) tensile specimens with different metallurgical conditions had been included in STIP I [3] and irradiated up to about 12 dpa with an average irradiation temperature range of 110–330 °C. In the following, we will present the results of tensile tests and Scanning Electron Microscope (SEM) fracture surface examinations conducted on 9Cr–1Mo and mod 9Cr–1Mo (T91 steel) specimens irradiated in the STIP II experiment up to 20 dpa and with a somewhat higher irradiation temperature range than was the case for STIP I.

2. Experimental details

2.1. Materials and specimens

The chemical compositions of the materials tested are provided in Table 1. The EM10 heat was identical to that used previously in the STIP I experiment [3]. Two types of miniature flat tensile specimens (so-called 'S' and 'L' specimens, whose dimensions are shown in Fig. 1) were

* Corresponding author.
E-mail address: jean.henry@cea.fr (J. Henry).

Table 1
Compositions of the steels (in wt%)

	C	Cr	Mo	V	Nb	Ni	Mn	N	P	Si
EM10	0.096	8.8	1.09	–	–	0.18	0.51	0.024	0.015	0.37
T91	0.105	8.26	0.95	0.2	0.075	0.13	0.38	0.0055	0.009	0.43

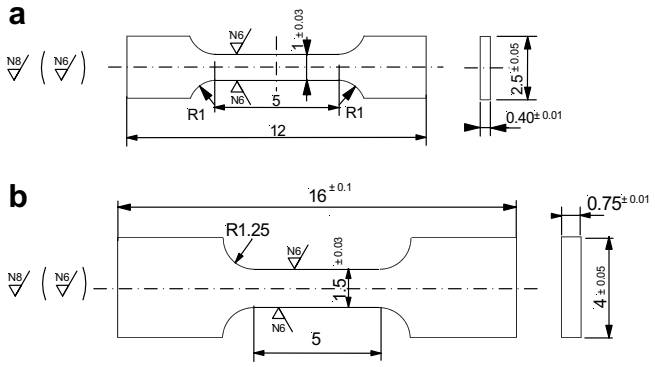


Fig. 1. Dimensions of the tensile specimens (in mm): (a) 'S' specimen (b) 'L' specimen.

machined from a 3.5 mm thick plate which had been normalized for 30 min at 980 °C, fast cooled, and tempered for 30 min at 750 °C. In the case of T91, only 'S' type specimens were prepared using a 3.5 mm thick plate which was in the 'standard' condition for the Phenix Reactor wrapper tubes, i.e. it had been subjected to the following heat treatment: normalized for 1 h at 1040 °C, fast cooled, tempered for 1 h at 760 °C, 20% cold worked and finally tempered for 1 h at 760 °C. After machining, the specimens were shipped to Paul Scherrer Institut (PSI) where they were laser-marked, placed together with other specimens in specimen holders and enclosed in tubes made of 316L austenitic stainless steel, as described in [2].

2.2. Irradiation conditions

The EM10 and T91 specimens were loaded in rod 1 and rod 3 whose locations are shown in Fig. 5 from [2]. The target was irradiated for 16 months starting in March 2000 and ending in December 2001, with an interrupt from January to May 2001. The total accumulated proton fluence was 10.03 Ah as compared to 6.3 Ah for the previous target. The proton and neutron fluences received by each specimen in the target and the corresponding dpa values and helium and hydrogen concentrations were calculated with the MCNPX code using the results of the gamma mapping performed on the beam entrance area of the $AlMg_3$ container, as explained in detail in [2]. Calculated neutron and proton fluences were compared to experimental values obtained from gamma spectra measurements of several dosimetry foils, using the same procedure as that used for STIP I [8]. The calculated values were found to be in relatively good agreement with experimental data, although slightly (10%) larger [12]. In addition, as in the case of STIP I [8], measurements of helium and hydrogen contents were performed by means of hot vacuum extraction in combination with gas mass spectrometry using discs of several materials located in the different specimen rods [2]. Depending on the positions of the discs in the specimen rods, the measured helium concentrations were 20–70% larger than the calculated values. The measured hydrogen values showed a strong dependence on the irradiation temperature of the specimens. The experimental values were much lower than the calculated ones for steel specimens irradiated at 250 °C or higher, which was attributed to diffusion of hydrogen at higher temperatures [8]. For the EM10 and T91 specimens, corrected helium values, based on the experimental data, are indicated in Table 2, together with the calculated dpa and hydrogen values. It should be noted that the hydrogen values are only an indication of hydrogen production during irradiation. The actual hydrogen concentrations retained in the specimens are not known.

The irradiation temperature of the specimens was not constant during the experiment, due to the fluctuation of the proton beam current. In addition to the frequent beam trips (about 50 per day), the average proton beam current fluctuated between 1 and 1.25 mA during the first 14 months and between 0.92 and 1.02 mA during the last two months, following a change in the beam line configuration. Furthermore, due to a slight overfocussing of the proton beam, the specimens experienced a high irradiation temperature for a period of 22 h in October 2000. However, the temperature excursion was significantly less severe than that which had occurred during the irradiation of the previous target [2,3].

The temperature of each specimen in the target was calculated as a function of total beam current using the ANSYS code as discussed in detail in [1,2]. The average irradiation temperature, the upper- and lower-bound temperatures experienced by each specimen during normal operation (excluding the beam trips) as well as the maximum temperature reached during the 22 h abnormal beam focussing are listed in Table 2.

2.3. Test conditions

The specimens were tensile tested using an Instron machine equipped with a furnace at an initial strain rate of $3 \times 10^{-4}\ s^{-1}$. The tests were conducted in air either at room temperature, 250 °C or 350 °C. Two specimens (one EM10 and one T91 specimen, irradiated to the highest dose) were annealed for 1 h at 750 °C and subsequently tested at room temperature. The recorded data were corrected for machine compliance in order to obtain for each specimen the engineering stress/engineering strain curve.

Table 2
Irradiation conditions and gas contents

Materials	Rod	ID mark	T_h[a] (°C)	T_l[b] (°C)	T_{av}[c] (°C)	T_{ex}[d] (°C)	dpa	He (appm)	H (appm)
EM10 'S' type	R1	G10	115	99	108	129	6.5	500	1950
	R1	G12	115	99	108	129	6.5	500	1950
	R3	G18	134	110	122	156	7.4	565	2050
	R3	G26	134	110	122	156	7.4	565	2050
	R3	G22	154	124	139	180	7.4	565	2050
	R1	G7	162	135	150	185	9.8	795	3250
	R1	G9	162	135	150	185	9.8	795	3250
	R1	G8	188	155	173	216	9.8	795	3250
	R3	G17	195	154	174	232	11.1	910	3440
	R3	G25	195	154	174	232	11.1	910	3440
	R3	G21	228	179	203	273	11.1	910	3440
	R1	G4	229	187	210	266	14.1	1205	4900
	R1	G6	229	187	210	266	14.1	1205	4900
	R1	G5	270	219	247	315	14.1	1205	4900
	R3	G16	277	214	245	333	15.8	1370	5300
	R3	G24	277	214	245	333	15.8	1370	5300
	R3	G20	328	252	290	397	15.8	1370	5300
	R1	G1	301	242	275	351	18.6	1645	6900
	R1	G3	301	242	275	351	18.6	1645	6900
	R1	G2	357	286	326	419	18.6	1645	6900
	R3	G15	348	266	307	423	19.8	1750	7400
	R3	G23	348	266	307	423	19.8	1750	7400
	R3	G19	415	316	366	506	19.8	1750	7400
EM 10 'L' type	R1	G35	136	115	127	154	7	550	2100
	R1	G36	136	115	127	154	7	550	2100
	R3	G3	160	129	145	189	7.9	615	2400
	R3	G42	160	129	145	189	7.9	615	2400
	R1	G33	220	180	203	255	11.8	980	3950
	R1	G34	220	180	203	255	11.8	980	3950
	R3	G2	269	208	239	324	13.4	1130	4600
	R3	G41	269	208	239	324	13.4	1130	4600
	R1	G31	335	269	306	393	17.9	1585	6680
	R1	G32	335	269	306	393	17.9	1585	6680
	R1	G1	393	299	346	479	19.3	1710	7180
	R1	G40	393	299	346	479	19.3	1710	7180
T91	R1	F1	123	105	115	139	7.2	565	2190
	R1	F3	123	105	115	139	7.2	565	2190
	R3	F17	127	105	116	147	7.2	535	2050
	R3	F13	142	116	129	166	7.2	535	2050
	R1	F2	141	119	131	160	7.2	565	2190
	R3	F18	180	144	162	213	10.7	850	3440
	R3	F14	205	162	183	244	10.7	850	3440
	R1	F4	176	146	163	202	11	920	3630
	R1	F5	206	169	189	238	11	920	3630
	R1	F6	176	146	163	202	11	920	3630
	R3	F19	259	201	230	312	15.2	1305	5300
	R3	F15	298	230	264	360	15.2	1305	5300
	R1	F7	255	207	233	296	15.9	1430	5730
	R1	F8	301	243	275	352	15.9	1430	5730
	R3	F20	335	256	295	405	19.6	1740	7400
	R3	F16	387	295	341	471	19.6	1740	7400
	R1	F10	320	257	292	375	19.9	1825	7600
	R1	F12	320	257	292	375	19.9	1825	7600
	R1	F11	382	305	347	448	19.9	1825	7600

[a] The upper-bound irradiation temperature.
[b] The lower-bound irradiation temperature.
[c] 'Average' irradiation temperature defined as $T_{av} = (T_h + T_l)/2$.
[d] Irradiation temperature during abnormal beam focussing.

Fracture surfaces of selected tensile specimens were analysed by scanning electron microscopy (SEM) using a JEOL 5400 microscope operated at a voltage of typically 15 kV.

Table 3
Tensile properties

Materials	ID mark	dpa	YS (MPa)	UTS (MPa)	UE (%)	TE (%)	T_{test} (°C)
EM10 'S' type	–	0	544	685	10.5	21.8	25
	–	0	588	688	8.4	18.4	25
	–	0	578	626	4.5	11.1	250
	–	0	512	582	6.4	12	350
	G10	6.5	989	995	0.35	7.5	25
	G12	6.5	797	808	0.4	7.6	250
	G18	7.4	777	797	0.4	6.7	250
	G26	7.4	1000	1007	0.45	7.3	25
	G22	7.4	1001	1002	0.18	7.0	25
	G7	9.8					
	G9	9.8	876	876	0.19	5.5	250
	G8	9.8	1116	1116	0.21	5.20	25
	G17	11.1	867	872	0.29	6.0	250
	G25	11.1	1120	1126	0.37	6.8	25
	G21	11.1	1074	1077	0.23	5.7	25
	G4	14.1	1207	1211	0.35	4.9	25
	G6	14.1	1262	1331	1.23	2.5	25
	G5	14.1	1140	1141	0.19	3.8	250
	G16	15.8	1280	1333	0.59	3.5	25
	G24	15.8	1212	1222	0.33	4.7	25
	G20	15.8	1090	1093	0.21	3.4	250
	G1	18.6	1267	1267	0.12	0.12	25
	G3	18.6	1095	1114	0.55	1.7	350
	G2	18.6	1093	1102	0.32	0.35	250
	G15	19.8	1256	1267	0.35	0.36	25
	G23[a]	19.8	1001	1047	5.6	11.8	25
	G19	19.8	1051	1063	0.65	3.8	350
EM 10 'L' type	–	0	317	568	58.9	67.4	25
	–	0	512	687	10.3	24.9	25
	–	0	510	613	6.7	19.5	250
	–	0	483	592	6.1	17.8	350
	G35	7	860	1022	0.98	11.8	25
	G36	7	849	857	0.54	11	250
	G3	7.9	1011	1021	0.43	11.5	25
	G42	7.9	784	805	0.56	11.5	250
	G33	11.8	1213	1225	0.43	6.3	25
	G34	11.8	1031	1049	0.56	5.9	250
	G2	13.4	1161	1163	0.27	7.93	25
	G41	13.4	946	951	0.38	7.6	250
	G31	17.9	1207	1223	0.32	0.33	25
	G32	17.9	1095	1111	0.75	5.3	250
	G1	19.3	1092	1092	0	0	25
	G40	19.3	1137	1137	0	0	25
T91	–	0	787	848	3.73	15.8	25
	–	0	621	697	3.66	10.1	250
	F1	7.2	1112	1117	0.37	6.97	25
	F3	7.2	906	929	0.75	7.46	250
	F17	7.2	875	894	1.0	7.38	250
	F13	7.2	1093	1100	0.5	6.72	25
	F2	7.2	1134	1138	0.28	6.87	25
	F18	10.7	1198	1207	0.36	6.69	25
	F14	10.7	1035	1045	0.45	6.39	250
	F4	11	1156	1187	0.49	7.1	25
	F5	11	1083	1088	0.24	4.9	250
	F6	11	1220	1224	0.25	5.53	25
	F19	15.2	1303	1314	0.34	5.63	25
	F15	15.2	1217	1223	0.33	3.6	250
	F7	15.9	1449	1458	0.31	0.36	25
	F8	15.9	1234	1252	0.43	2.47	250
	F20	19.6	1451	1455	0.21	0.21	25
	F16	19.6	1209	1234	0.35	0.4	350
	F10[a]	19.9	1168	1209	4.48	7.74	25
F12	19.9	1408	1419	0.44	0.53	25	
F11[b]	19.9	–	–	–	–	–	

[a] Specimen annealed for 1 h at 750 °C prior to testing.
[b] Specimen broke during mounting.

3. Results

3.1. Tensile tests

The tensile data for all tested specimens are listed in Table 3 and plotted in Figs. 10–15. Representative stress/strain curves are shown in Figs. 2–9. As expected for 9Cr martensitic steels irradiated at low temperatures to doses above 6 dpa, all specimens tested at room temperature exhibited marked hardening and loss of ductility: the irradiated specimens displayed values of uniform elongation of less than 1%. In addition, there was a change in the tensile

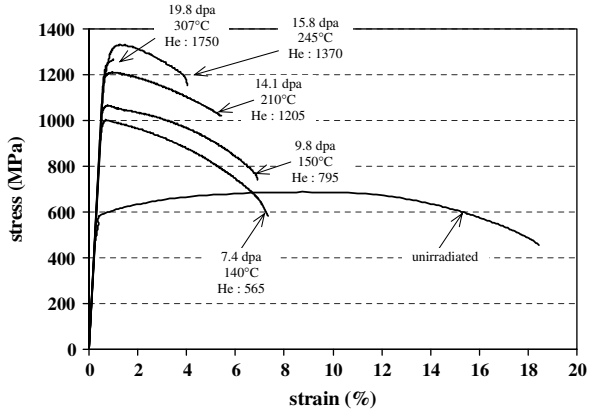


Fig. 2. Examples of stress/strain curves for EM10 'S type' specimens tested at room temperature. For each curve, the dose, helium content in appm and average temperature (as defined in Table 2) are indicated.

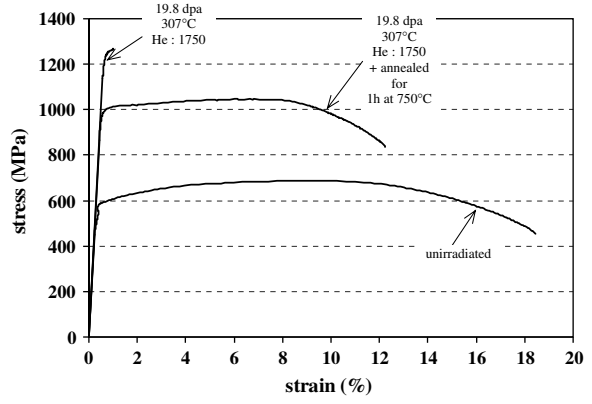


Fig. 3. Tensile curve measured at room temperature for a EM10 specimen (S geometry) annealed following irradiation compared to the 'as-irradiated' curve.

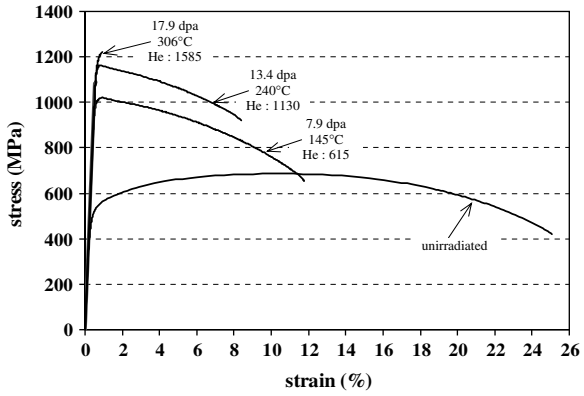


Fig. 4. Selected tensile curves for EM10 'L type' specimens tested at room temperature. For each curve, the dose, helium content in appm and average temperature (as defined in Table 2) are indicated.

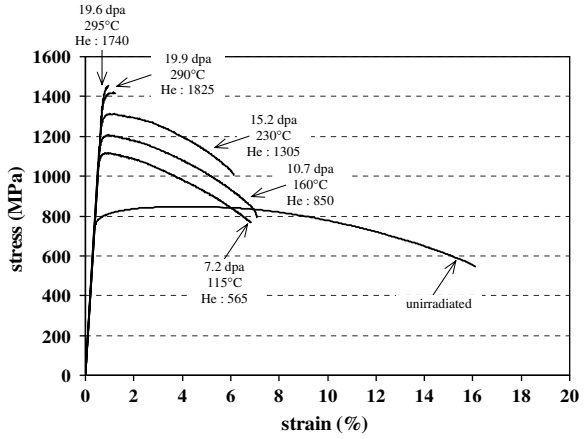


Fig. 5. Examples of stress/strain curves for T91 specimens tested at room temperature. For each curve, the dose, helium content in appm and average temperature (as defined in Table 2) are indicated.

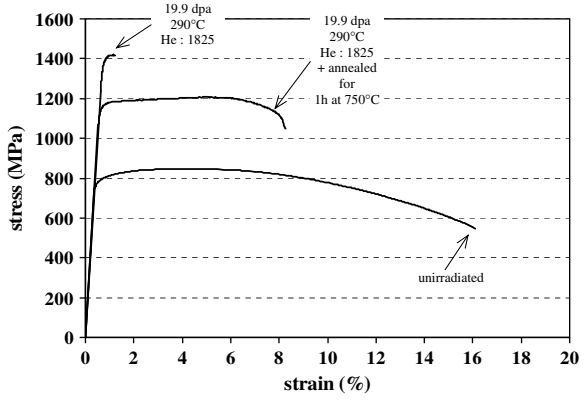


Fig. 6. Tensile curve measured at room temperature for a T91 specimen annealed following irradiation compared to the 'as-irradiated' curve.

behaviour at doses above about 15–16 dpa. The specimens irradiated to the highest doses broke either at yield with almost no plastic deformation (EM 10 'S' type specimens G1 and G15; 'L' type specimens G31, T91 specimens F20

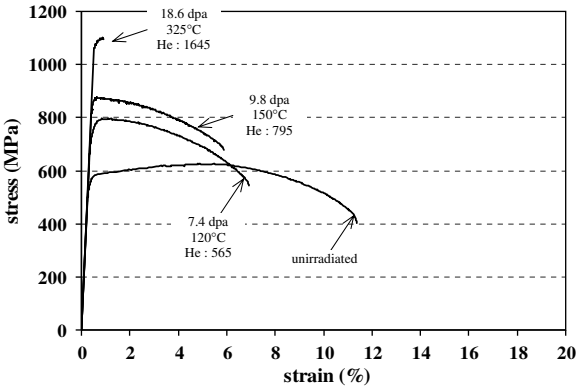


Fig. 7. Examples of stress/strain curves for EM10 'S type' specimens tested at 250 °C. For each curve, the dose, helium content in appm and average temperature (as defined in Table 2) are indicated.

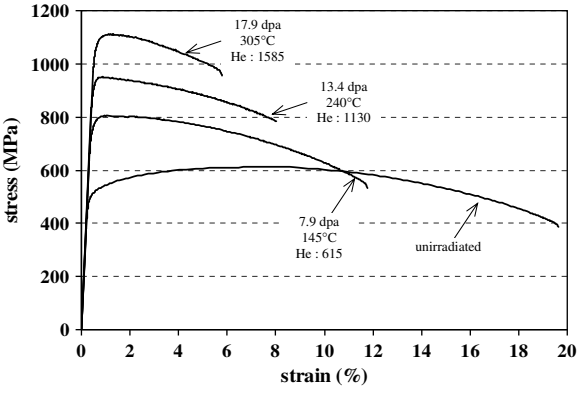


Fig. 8. Selected tensile curves for EM10 'L type' specimens tested at 250 °C. For each curve, the dose, helium content in appm and average temperature (as defined in Table 2) are indicated.

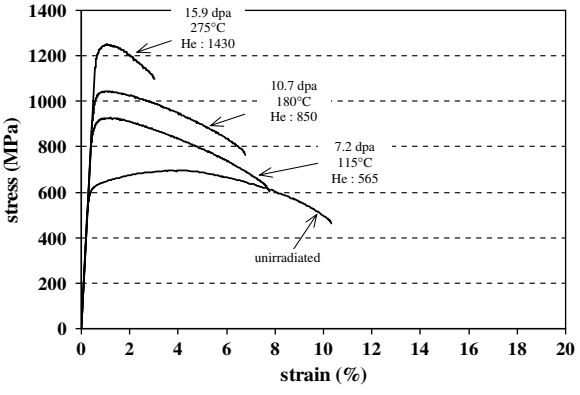


Fig. 9. Examples of stress/strain curves for T91 specimens tested at 250 °C. For each curve, the dose, helium content in appm and average temperature (as defined in Table 2) are indicated.

and F12, see Table 3) or broke during the elastic regime (EM10 'L' specimens G1 and G40).

The evolution of the tensile properties measured at 250 °C and 350 °C was similar to that observed at room temperature, although the brittle behaviour displayed at

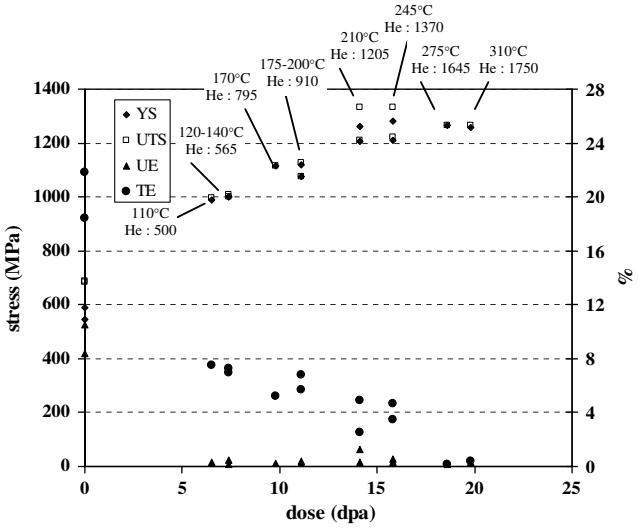


Fig. 10. Tensile properties (YS: yield stress; UTE: ultimate tensile strength; UE: uniform elongation; TE: total elongation) as a function of dose measured at room temperature on EM10 tensile specimens ('S' type). For each set of data points, Helium content and average irradiation temperature are indicated (in some cases, two samples with identical doses and different temperatures were tested).

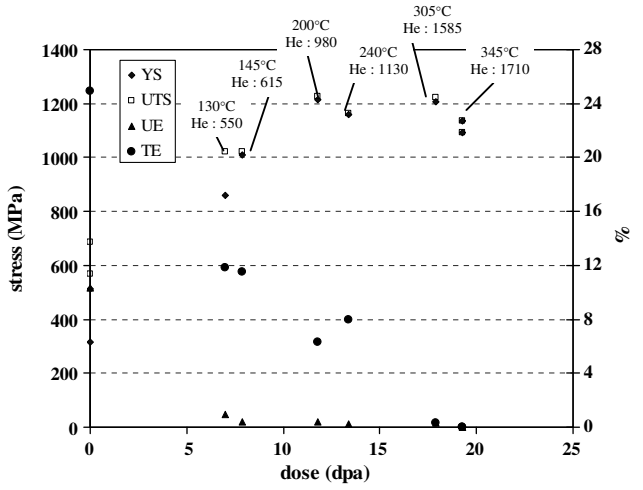


Fig. 11. Tensile properties (YS: yield stress; UTE: ultimate tensile strength; UE: uniform elongation; TE: total elongation) as a function of dose measured at room temperature on EM10 tensile specimens ('L' type). For each set of data points, Helium content and average irradiation temperature are indicated.

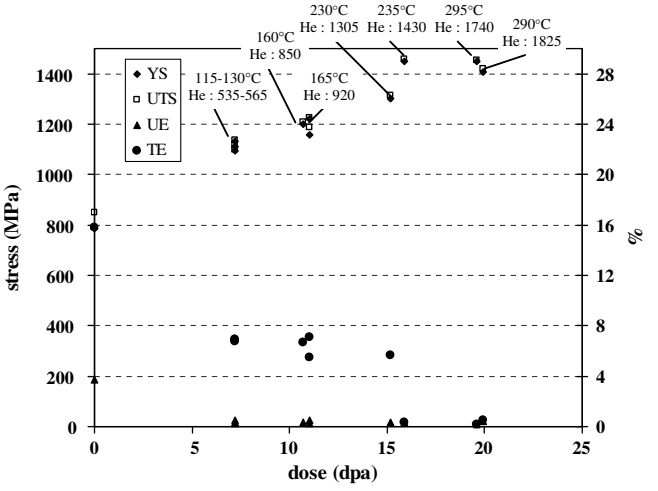


Fig. 12. Tensile properties (YS: yield stress; UTE: ultimate tensile strength; UE: uniform elongation; TE: total elongation) as a function of dose measured at room temperature on T91 tensile specimens. For each set of data points, Helium content and average irradiation temperature are indicated (in some cases, up to three samples with identical doses and different temperatures/helium contents were tested).

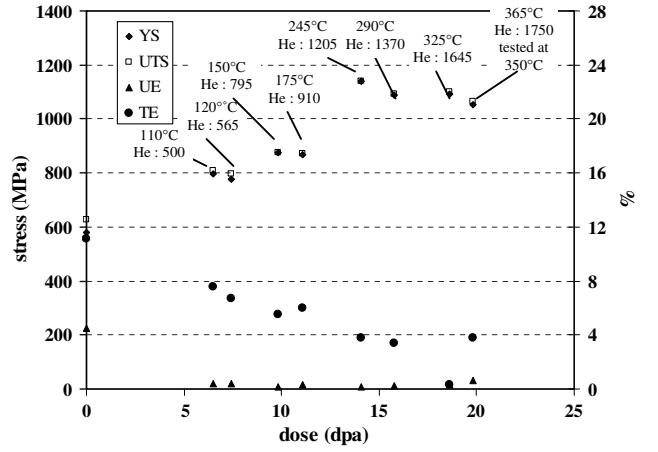


Fig. 13. Tensile properties (YS: yield stress; UTE: ultimate tensile strength; UE: uniform elongation; TE: total elongation) as a function of dose measured at 250 °C on EM10 tensile specimens ('S' type). For each set of data points, Helium content and average irradiation temperature are indicated (in some cases, two samples with identical doses and different temperatures were tested). The data points for one sample irradiated at the maximum dose and tested at 350 °C are also plotted.

room temperature by the specimens irradiated to the highest doses was not systematically observed at higher test temperatures. For instance while specimen G2 (EM10, 'S' type specimen) irradiated to 18.6 dpa broke at yield when tested at 250 °C, specimen G32 (EM10 'L' type specimen) irradiated to 18 dpa exhibited some plastic deformation. The EM 10 specimens ('S' geometry) irradiated to 18.6 dpa (specimen G2) and 19.8 dpa (G19) both tested at 350 °C showed some plastic deformation whereas for the same test temperature, T91 specimen F16 irradiated to 19.6 dpa broke at yield.

Finally, the annealing treatment had a remarkable effect on the tensile properties. Fig. 3 (EM10 steel) and 6 (T91) show the tensile curves for an irradiated sample and for a sample irradiated side-by-side and annealed prior to testing. For both steels, the heat treatment induced a very significant recovery of the ductility and strain-hardening capacity, almost back to the values corresponding to the unirradiated materials. In addition, although there was a decrease in hardening compared to the as-irradiated samples, the annealed specimens displayed values of yield stress about 400 MPa above those of the unirradiated steels.

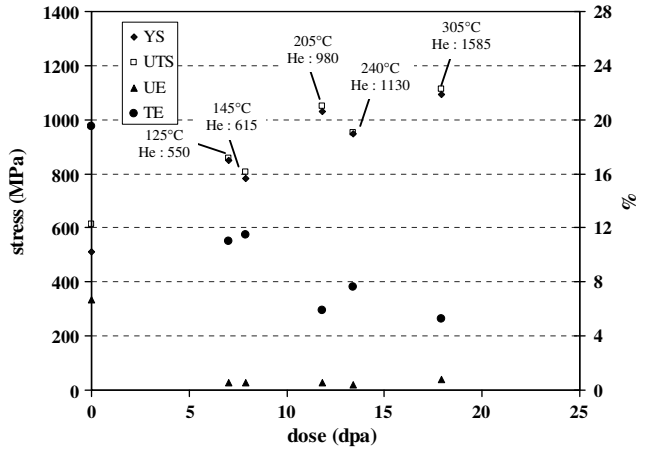


Fig. 14. Tensile properties (YS: yield stress; UTE: ultimate tensile strength; UE: uniform elongation; TE: total elongation) as a function of dose measured at 250 °C on EM10 tensile specimens ('L' type). For each set of data points, Helium content and average irradiation temperature are indicated.

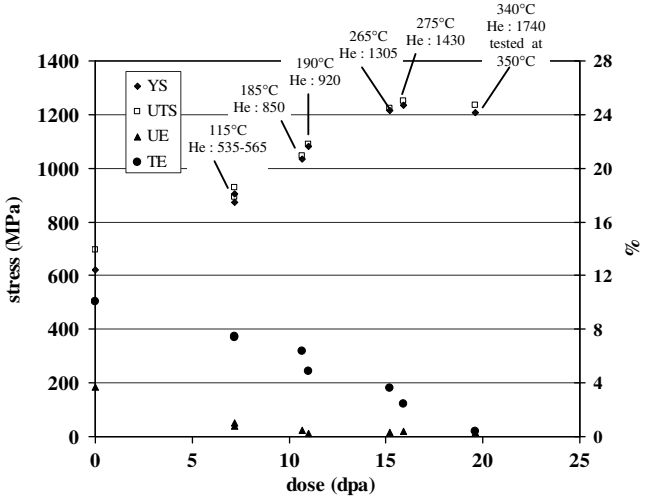


Fig. 15. Tensile properties (YS: yield stress; UTE: ultimate tensile strength; UE: uniform elongation; TE: total elongation) as a function of dose measured at 250 °C on T91 tensile specimens. For each set of data points, Helium content and average irradiation temperature are indicated (in one case, two samples with identical doses and different helium contents were tested). The data points for one sample irradiated at the maximum dose and tested at 350 °C are also plotted.

3.2. SEM observations

SEM observations were performed on the fracture surfaces of selected specimens irradiated to doses above 15 dpa. The observations showed that for all specimens tested at room temperature (Figs. 16–21), fracture occurred without necking. The fracture surfaces were found to be flat and perpendicular to the specimen axis with a fully brittle appearance. It can be noted that failure occurred in the fillet, i.e. outside the gauge section, for both EM10 'L' samples (Figs. 18 and 19). The fracture mode was intergranular separation (on average, the intergranular areas made up more than 50% of the fracture surfaces) and quasi-cleavage. The percentage of intergranular areas tended to be greater at the centre of the specimens, while the amount of quasi-cleavage increased at the periphery of the fracture surfaces. The intergranular separation obviously occurred along former austenitic grain boundaries, as evidenced by the larger grain sizes on the fracture surfaces of EM10 specimens compared to the grain sizes on T91 fracture surfaces.

The fracture surfaces of the samples tested at higher temperatures were more diverse. EM10 G2 specimen irradiated to 18.6 dpa and tested at 250 °C broke without necking in a brittle manner (Fig. 22). However, the amount of intergranular area was less than what was measured on specimens tested at room temperature. In addition, a few areas with a ductile appearance were also detected. T91 specimen F15 was irradiated to a lower dose (15 dpa). It was tested at 250 °C and displayed some necking before failure (Fig. 23). The fracture surface was rather flat with a ductile appearance in the centre and, closer to the edges, some secondary cracks were present. EM10 specimen G19, irradiated to 19.8 dpa and tested at 350 °C also exhibited some necking (Fig. 24). There were numerous secondary cracks on the fracture surface, some of which seemed to follow grain boundaries. However the fracture appearance was ductile, with well formed dimples. By contrast, in the case of T91 specimen irradiated to 19.6 dpa and also tested at 350 °C, fracture occurred without necking (Fig. 25). The fracture appearance was fully brittle, with both intergranular failure mode (about 60% of the fracture surface) and quasi-cleavage. It can be mentioned however that, contrary to the case of the specimens tested at room temperature, a few ductile zones with the presence of dimples were also detected.

4. Discussion

Fig. 26 presents the increase in yield stress for the EM10 samples irradiated in STIP II as function of displacement damage. For comparison, the data obtained for the same heat of material and identical metallurgical condition following irradiation in the STIP I experiment, irradiation in the mixed-spectrum Osiris [4] and SM2 reactors [5] are plotted as well. This figure shows that there is a good agreement between the STIP I and STIP II data except for one STIP I data point at 11.4 dpa, which lies below the general data trend: the reason for this apparent abnormal behaviour is discussed below. The specimens irradiated in STIP II display high hardening at doses above 10 dpa. This may be an effect of the spallation environment which generates large quantities of gases in the specimens. However, it must be pointed out that the same level of hardening was measured following irradiation to 14 dpa in the SM2 reactor (SAMARA experiment [5], see Fig. 26). On the other hand, an important result of the present experiment is the brittle behaviour and intergranular fracture mode displayed by the EM10 and T91 specimens irradiated at high

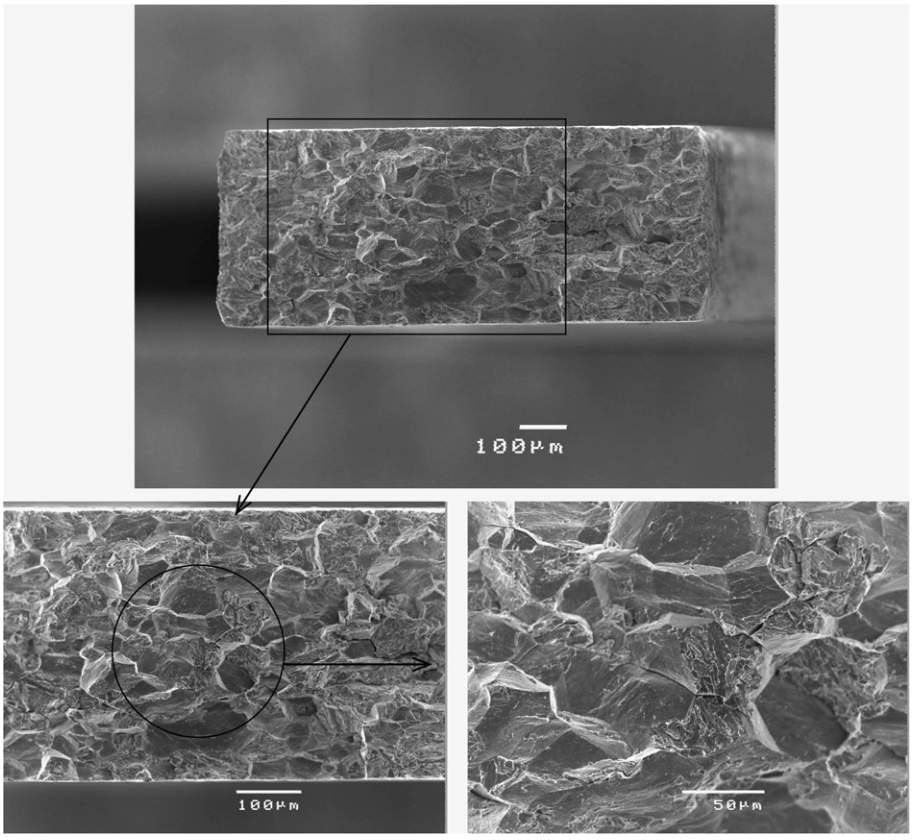


Fig. 16. SEM micrographs showing the fracture surface of EM10 specimen G1 ('S' type) irradiated to 18.6 dpa and tested at room temperature.

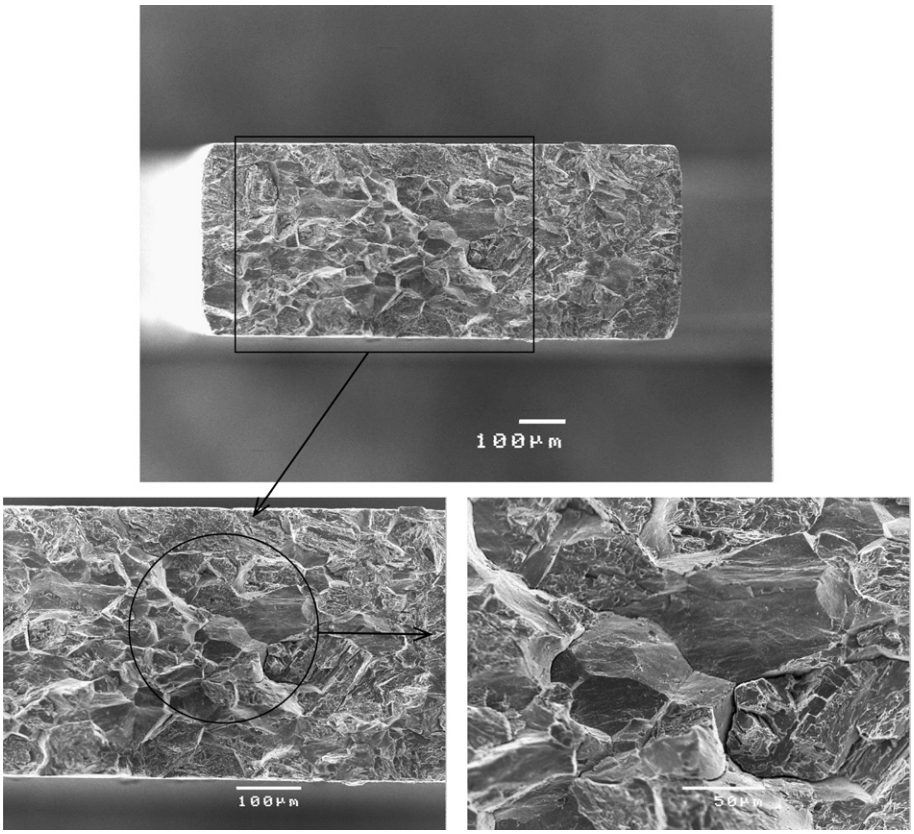


Fig. 17. SEM micrographs showing the fracture surface of EM10 specimen G15 ('S' type) irradiated to 19.8 dpa and tested at room temperature.

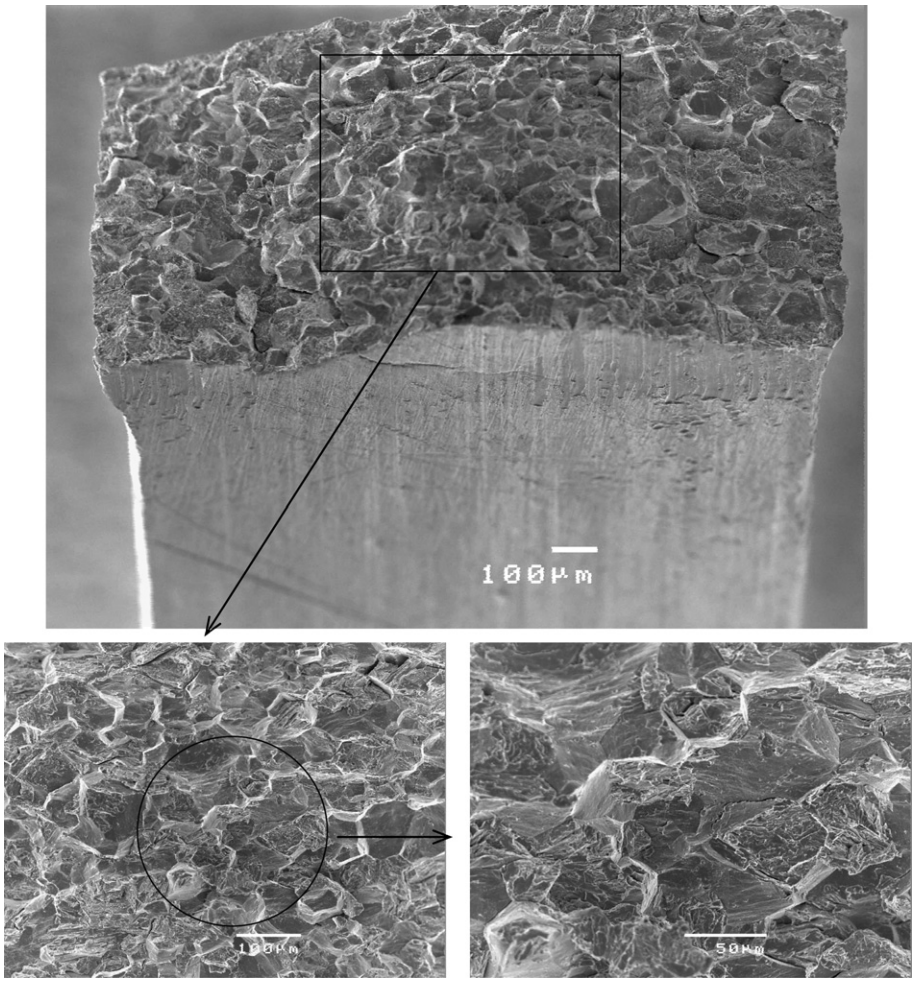


Fig. 18. SEM micrographs showing the fracture surface of EM10 specimen G31 ('L' type) irradiated to 17.9 dpa and tested at room temperature.

dose in the STIP II experiment, whereas the specimens irradiated in the SM2 reactor broke in a ductile manner. Such a fracture mode was never observed up to now in tensile tests performed on martensitic steels in the standard metallurgical condition irradiated in fission or spallation environments. Recent bending tests performed at room temperatures on T91 specimens implanted up to 1250 and 2500 appm He at both 250 °C and 400 °C [6,7] have demonstrated that helium induces a decrease in the critical stress for intergranular fracture. Therefore, the intergranular fracture mode may be due to the high helium concentrations (up to about 0.18 at.% appm, see Table 2) in the specimens irradiated to the higher doses. Hydrogen effects are probably not significant, since measurements by Dai et al. [8] performed on specimens irradiated in STIP I have shown that for irradiation temperatures above 200 °C most of the produced hydrogen escapes, whereas helium is retained.

The other noteworthy result of the present work is the drastic change of tensile behaviour following post-irradiation annealing of the EM10 and T91 specimens irradiated to about 20 dpa. In fact the tensile curves measured after annealing are very similar to those measured on EM10 samples in both 20% cold work and normalised and tempered metallurgical conditions irradiated to 11.4 dpa in the STIP I experiment [3]. Compared to samples irradiated to lower doses, these specimens displayed a 'recovery' of the strain-hardening capacity associated with a large increase of uniform and total elongation together with a lower yield stress value, which remained nevertheless significantly above that of the unirradiated materials. The same phenomenon was recently observed for different ferritic/martensitic steels irradiated in STIP I [9]. It was suggested [3] that this 'recovery' of ductility was due to the fact that during the STIP I irradiation, the target was hit by a focussed beam: as a consequence, some specimens presumably reached high temperatures. The results of the present annealing experiment support this hypothesis.

In a previous study, Chen et al. [10] had performed tensile tests on a 11Cr martensitic steel irradiated in a spallation environment at LANSCE to about 6 dpa and 1300 appm He and subsequently annealed for 1 h at 700 °C. Jung et al. [11] also measured the tensile properties of 9Cr Eurofer implanted with 0.25 at.% He at 250 °C and annealed at 750 °C for 10 h. In both cases, as observed in the present work, the ductility and strain-hardening

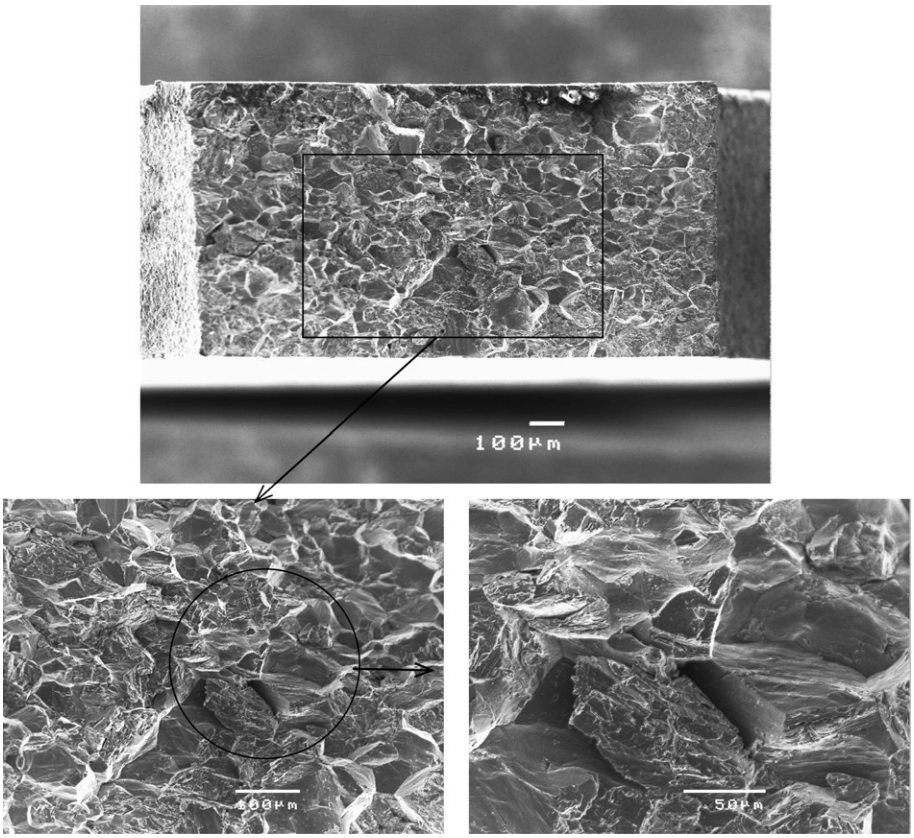


Fig. 19. SEM micrographs showing the fracture surface of EM10 specimen G1 ('L' type) irradiated to 19.3 dpa and tested at room temperature.

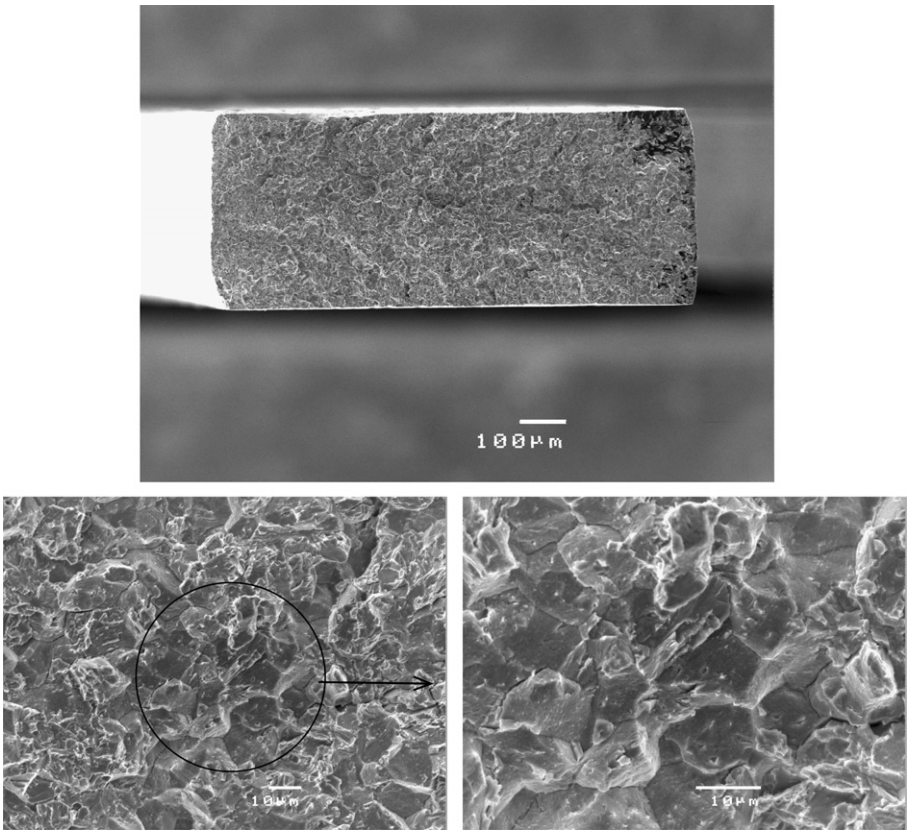


Fig. 20. SEM micrographs showing the fracture surface of T91 specimen F20 irradiated to 19.6 dpa and tested at room temperature.

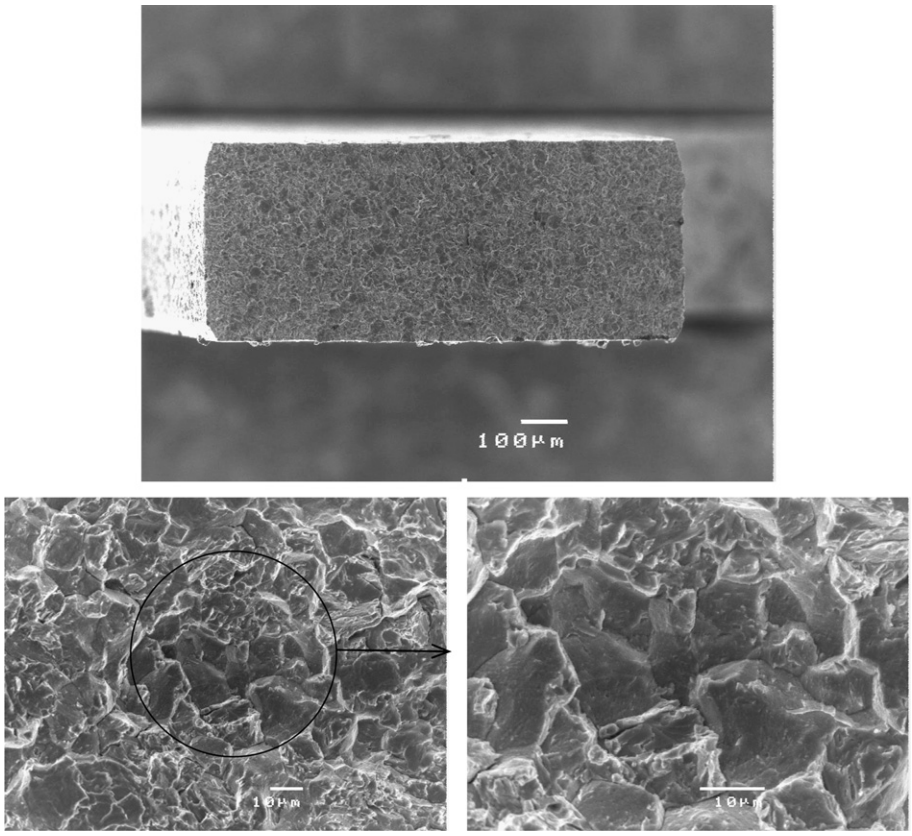


Fig. 21. SEM micrographs showing the fracture surface of T91 specimen F12 irradiated to 19.9 dpa and tested at room temperature.

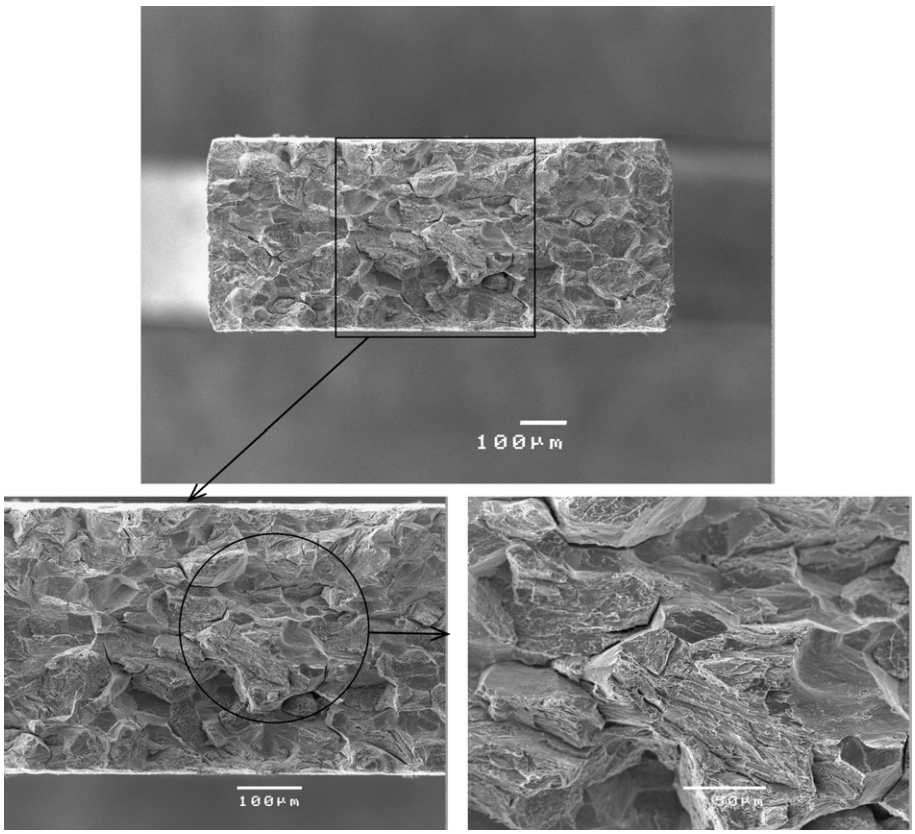


Fig. 22. SEM micrographs showing the fracture surface of EM10 specimen G2 ('S' type) irradiated to 18.6 dpa and tested at 250 °C.

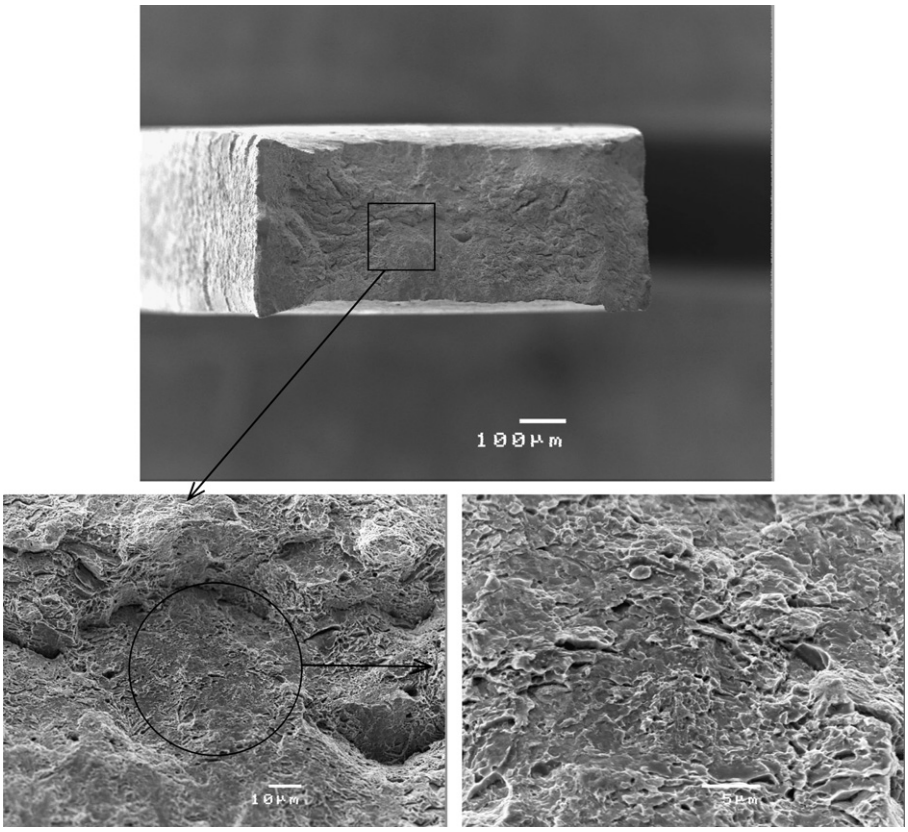


Fig. 23. SEM micrographs showing the fracture surface of T91 specimen F15 irradiated to 15.2 dpa and tested at 250 °C.

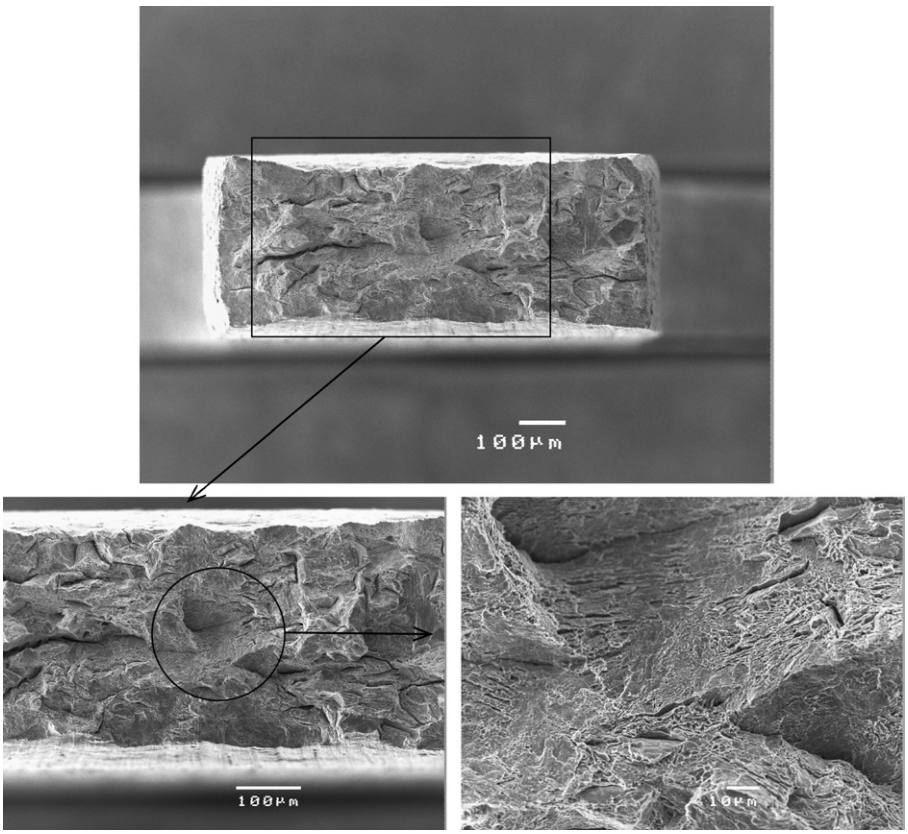


Fig. 24. SEM micrographs showing the fracture surface of EM10 specimen G19 ('S' type) irradiated to 19.8 dpa and tested at 350 °C.

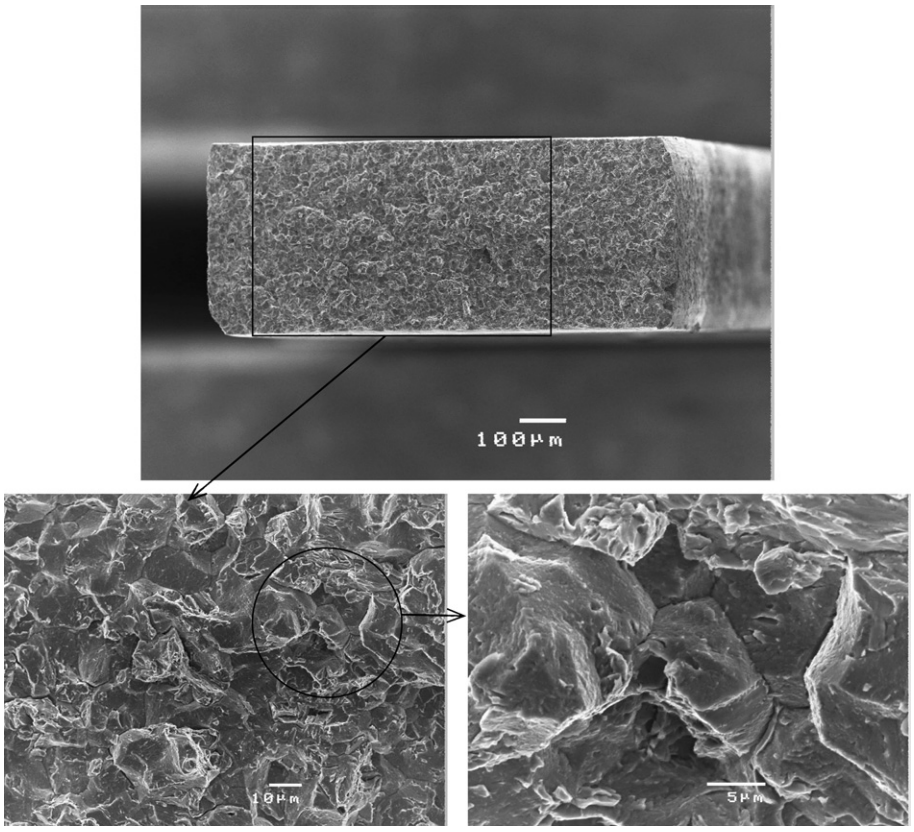


Fig. 25. SEM micrographs showing the fracture surface of T91 specimen F16 irradiated to 19.6 dpa and tested at 350 °C.

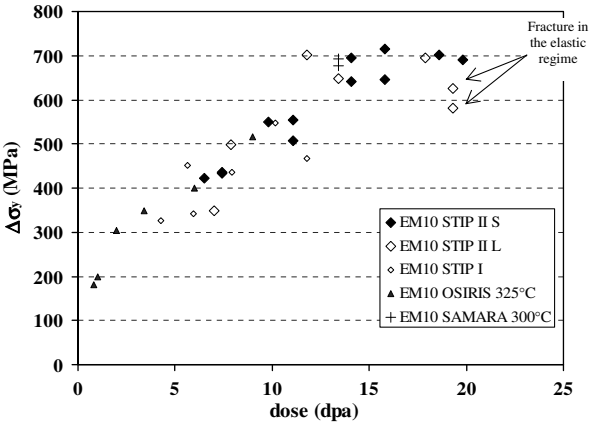


Fig. 26. Increase in yield stress as a function of dose for the EM10 specimens in the Normalised and Tempered metallurgical condition after exposure in a spallation environment (STIP II and STIP I [3] irradiations) or with fission neutrons (irradiations in the OSIRIS [4] and SM2 [5] thermal reactors). The data points indicated by arrows were calculated as the difference between the fracture stress following irradiation and the yield stress of the unirradiated steel since the specimens broke in the elastic regime.

capability recovered almost back to the initial values while the hardening was moderately reduced compared to the as-irradiated condition. In order to explain the tensile behaviour following annealing of spallation-irradiated or helium implanted samples, detailed microstructural investigations are necessary. In particular, the characterization of the dislocation microstructures which result from the annealing of the point defect clusters and measurements of dislocation/helium bubble densities and bubble size distributions should be carried out. Based on such data, it should be possible to decide whether the high retained hardening and ductility recovery after annealing are due primarily to an increase of the dislocation density compared to the unirradiated condition, as proposed in [11], or to the presence a high density of tiny helium bubbles.

5. Conclusions

The tensile behaviour of two 9Cr–1Mo tempered martensitic steels were measured following irradiation in the STIP II experiment. The evolution of the tensile properties with dose was very similar to that observed on the EM10 specimens irradiated in STIP I. The interesting finding of the present study is the change in fracture behaviour at doses above about 16 dpa. While the specimens irradiated at lower doses exhibited a ductile fracture mode, the high dose samples were brittle and some broke in the elastic regime. Significant amounts of intergranular separation (more than 50% of the fracture surfaces) were detected. It is suggested that the change of fracture behaviour of the high dose specimens may be due in particular to the high helium concentrations in those specimens. Increasing the test temperature to 250 °C did not improve significantly

the ductility of the specimens irradiated to the highest doses. The EM10 specimen irradiated to about 20 dpa showed some ductility when tested at 350 °C, while the T91 specimen irradiated to the same dose exhibited a brittle behaviour.

Both T91 and EM10 specimens irradiated to 20 dpa showed an important recovery of ductility following annealing, with improved strength compared to the unirradiated materials. The present results and those of earlier studies [10,11] show that heat treatment of structural parts of spallation devices should be seriously envisaged. Of course, the optimum heat treatment conditions still have to be determined and the effect of reirradiation following annealing needs to be assessed.

Acknowledgement

The work presented here was supported by the EUROTRANS project (6th European Framework Programme, Contract number FI6W-CT2005-516520).

References

[1] Y. Dai, G.S. Bauer, J. Nucl. Mater. 296 (2001) 43.
[2] Y. Dai, X. Jia, R. Thermer, D. Hamaguchi, K. Geissmann, E. Lehmann, H.P. Linder, M. James, F. Gröschel, W. Wagner, G.S. Bauer, J. Nucl. Mater. 343 (2005) 33.
[3] J. Henry, X. Averty, Y. Dai, P. Lamagnère, J.P. Pizzanelli, J.J. Espinas, P. Wident, J. Nucl. Mater. 318 (2003) 215.
[4] Y. de Carlan, X. Averty, J.C. Brachet, J.L. Bertin, F. Rozenblum, O. Rabouille, A. Bougault, Effects of Radiation on Materials: 22nd International Symposium, 8–10th June 2004, Boston, USA.
[5] A. Alamo, J.-L. Bertin, V.K. Shamardin, P. Wident, J. Nucl. Mater. 367–370 (2007) 54.
[6] J. Henry, L. Vincent, X. Averty, B. Marini, P. Jung, J. Nucl. Mater. 356 (2006) 78.
[7] J. Malaplate, L. Vincent, X. Averty, J. Henry, B. Marini, Eng. Fract. Mech. (in press).
[8] Y. Dai, Y. Foucher, M.R. James, B.M. Oliver, J. Nucl. Mater. 318 (2003) 167.
[9] Y. Dai et al., J. Nucl. Mater. 377 (2008) 115.
[10] J. Chen, P. Jung, M. Rödig, H. Ullmaier, G.S. Bauer, J. Nucl. Mater. 343 (2005) 227.
[11] P. Jung, J. Chen, H. Klein, J. Nucl. Mater. 356 (2006) 88.
[12] Y. Dai, M. James, F. Hegedus (submitted for publication).